High Resolution Beam Tomography on 3D Land Data Applications

Abdulmohsen AlAli, Ramzy Alzayer and Constantinos Tsingas, Saudi Aramco; Nick Tanushev and Alexander Mihai Popovici, Z-Terra Inc*

Summary

Velocity-depth model building is the most critical and resource demanding task in seismic imaging. Therefore, an efficient velocity-depth model building technique can significantly expedite subsequent decision making. The automated Beam Tomography is a super-efficient velocity model building methodology that allows faster turnaround than conventional driven reflection tomography while preserving the velocity model accuracy. We investigate the efficiency of the Beam Tomography technique on two 3D seismic datasets, acquired using conventional acquisition (nonblended) and simultaneous shooting acquisition (blended) with variable noise and complexity.

Introduction

Building a depth velocity model is a laborious but essential step to depth imaging in areas with large lateral variations in topography, complex geology and near-surface velocity heterogeneities. FWI (Tarantola, 1984; Virieux and Operto, 2009) and Conventional Migration Velocity Analysis methods (MVA) (Al-Yahya, 1989; Biondi and Sava, 1999; Sava et al., 2005; Albertin et al., 2006) are well established techniques to build velocity depth models. However, FWI is prone to the infamous "cycle-skipping" problem due to lack of a low-frequency component of the data and MVA requires significant resource allocation and human interaction.

Beam tomography is the combination of Fast Beam Migration (FBM) with an optimized Beam-domain Reflection Tomography (BRT). FBM is faster than conventional Kirchhoff migration via beam forming of the input data where the traces are converted into beams representing locally coherent events characterized by an arrival time, source and receiver locations, amplitude, dip orientation and curvature (Fomel and Tanushev, 2009). The beams are used to image the subsurface and subsequently their residual moveout assists in updating the velocity model. The accuracy of the beam based methods is controlled by the beam forming parameter, or, equivalently, by an initial beam width at the surface (Červený et al., 1982; Weber, 1988; Hill, 2001).

Beam-domain Reflection Tomography replaces the conventional steps in reflection tomography, such as, picking of residual moveout and semblance analysis by automated 3D residual time shifts in the beam domain. In the beam-imaging stage, the wavelet is spread locally near the imaging point. The residual time shifts are used to vary the beam wavelet spreading in the image space if the travel time along the source and receiver rays were longer or shorter (Tanushev et al., 2017). This results in shifting the beam image in the direction perpendicular to the reflector that the beam is imaging.

Converting those shifts into local velocity perturbation allow us to build an azimuthally dependent tomographic solution. The velocity-depth model is updated along each of the ray paths with certain constraints to obtain an updated subsurface image. After a number of iterations, Beam Tomography converges to a final velocity-depth model allowing the user to fine tune the parameters on the fly without significant intervention (Tanushev et al., 2017). Figure 1 shows a comparison between a conventional and a Beam Tomography velocity update workflow.

Results and Discussion

Conventional Data:

In the first application, the target is a dipping four-way closure structure with a complex near surface. The acquisition was based on a distance separated field configuration where the sources obeyed a specific time-distance rule. It was an orthogonal geometry in which the source line spacing is 250 m, receiver line spacing was 125 m and the source and receiver station interval was 25 m. The data went through a conventional processing workflow and an interval velocity – depth model was derived using a Constrained Velocity Inversion (CVI) algorithm.

We obtained a velocity model that produces flat FBM angle gathers and a corrsponding update that reflects the closure structure after 14 iterations. Figure 2 shows a comparison at two check-shot locations between Beam Tomography driven model from CVI and the accepted Kirchhoff-reflection tomography driven model. The Beam Tomography updated velocity model matched the check-shots trend, highlighting key interfaces in the velocity model. The higher resolution observed on the Beam Tomography solution is attributed to the unique moveout residual computation coupled with a small inversion grid size.

We used Kirchhoff prestack depth migration to image the data using the velocity obtained from the 14th iteration of Beam Tomography and benchmarked it against that from an existing Kirchhoff-reflection-Tomography model. The quality of the two offset image gathers shown in Figure 3 is comparable throughout the survey. The depth stacks are depicted in Figure 4 with well markers highlighting horizons of interest. The estimated depth for both horizons is extremely close.

Overall, the results show pristine structure images highlighting distinct faults and geological features of interest. The full Beam Tomography solution is achieved in 14 days compared to few months for the conventional Kirchhoff Reflection Tomography solution. The turnaround time can be utilized for more sophisticated velocity analysis such as anisotropic parameter estimation to further improve the structural imaging.

We further challenge the method's validity in building a reliable velocity model by comparing the results of the CVI driven model and a constant velocity model (average of CVI) in the Beam Tomography loop. Figure 5a shows a comparison between the Beam tomography solution driven from the CVI 14th iteration vs constant 12th iterations velocity models. Despite the unrealistic constant starting velocity model, both solutions match the shallower trend observed on the check-shot. The CVI driven model has superior accuracy in the deeper section due to a more accurate starting model.

Figure 5b shows the L2 norm of the residual error across a single inline per iteration on the two models. It represents a qualitative measure of how the residual error in both solution behaves for each iteration. The CVI model converges with each iteration and no significant changes are made after the 9th iteration. The constant velocity, fluctuates between converging and diverging in the first few iterations and finally it shows an overall convergence after the 9th iteration.

Simultaneous acquisition Data:

In the second application, the target is prominent low offset faults. The near surface has a distinct high velocity zone that complicates the accurate imaging of deeper formations. The data are acquired through an unconstrained and decentralized blended acquisition survey, namely, 3D Dispersed Source Array (DSA) (Tsingas et al., 2020). An orthogonal acquisition geometry was employed in which the source and receiver line spacing was 75 m and the source and receiver station interval was 25 m. The DSA is a decentralized blended acquisition technology were multiple sources are firing almost simultaneously resulting in the collection of a high density broadband blended data. This acquisition methodology significantly shortens the operational time while improves the frequency content and increases data density.

There is significant amount of crosstalk noise generated due to the simultaneous acquisition. Deblending methods to suppress crosstalk are time-consuming as they require manual parametrization or expensive data-driven inversion solutions to obtain acceptable results (Richardson and Feller, 2019). Tsingas et al. (2020) presented full details on the processing workflow using novel techniques to deblend the data. We carry Beam Tomography on both raw blended data (no processing) and deblended processed data in order to examine the robustness of Beam Tomography workflow in the presence of crosstalk noise.

Nine (9) iterations were needed for the processed data vs ten (10) iterations for the raw blended data to produce flat FBM angle gathers and a corresponding velocity model that reflects the high velocity zone (Figure 6). Illumination on the edges of the survey was an issue for both data sets due to low acquired fold. Despite the high crosstalk noise recorded in the blended data, the source and receiver beam generation indirectly suppressed its impact on the beam formed data prior to tomography. The noise in the far offset (shallower than the reflection) can still generate a noise-dominant beam that still leaks into the data.

We use Kirchhoff depth migration to image and stack the raw and processed data using their respective updated velocities. Figure 7 shows the offset image gathers with key reflectors marked to comparable depths. Figure 8 shows the stacks with the low offset faults zone highlighted on both depth stacks. The belnded depth stack shows more continuous events in the shallow section mirroring the continuity seen on the offset gathers.

Next, we compare the two velocities with an offset check-shot (Figure 9a). The offset check-shot does not start from the surface. A section of the check-shot correlates well with the trend seen on both velocity models. No significant update was made on the deeper section due to illumination limitations of the survey (lack of far offsets). The illumination challenges is better described in Figure 9b and 9c where we illustrate the beam migration stack co-rendered by the illumination i.e., a measure of how many beams have been used to image/update a point in the subsurface. Multiple factors control the illumination, namely: the acquisition design, the shallow velocity anomaly that makes it difficult to image the deeper section as well as data processing. The arrows on the stack and check-shot show similar depth points.

Conclusions

Beam Tomography is the combination of Fast Beam migration with an automated Beam Domain tomography that allows a significant fast turnaround time for 3D land seismic depth imaging projects expediting the laborious manual components of velocity-depth model building. We have demonstrated using two datasets the efficiency of the method on a conventionally acquired data building a highly accurate velocity model. A second demonstration has shown the efficiency of the method to build a velocity model on blended data with desirable accuracy.

As a novel approach, Beam Tomography increases the reliability and estimation of target-oriented velocity model updates and the corresponding depth images, which allow interpreters to assess various preliminary depth images and even make decisions during acquisition time. Beam Tomography paves the way for almost real time depth imaging application impacting acquisition geometries, which in turn can be beneficial for infill acquisition to mitigate illumination artifacts.

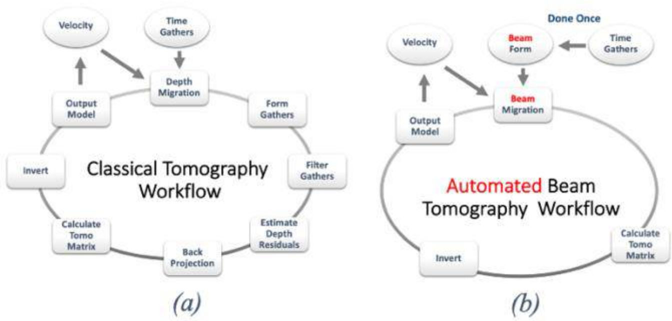

Figure 1(a) Conventional velocity model building workflow. (b) Automated Beam Tomography workflow.

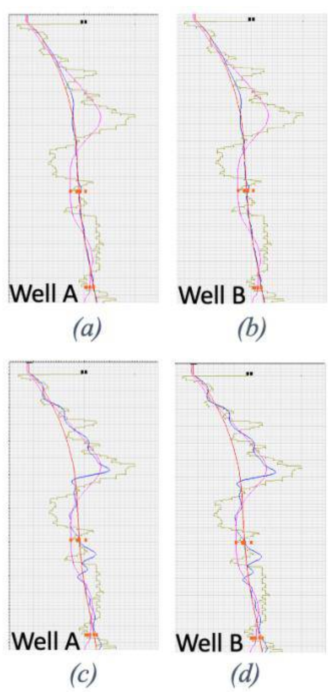

Figure 2. Gold: Check-shot. Red: Starting Velocity model. Blue: Beam Tomography. Pink: Archived Kirchhoff reflection tomography built velocity model. (a) and (b) Beam Tomography iterations 1. (c) and (d) Beam Tomography iteration 15.

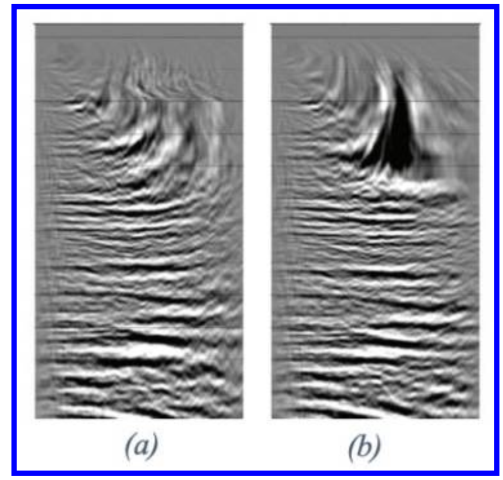

Figure 3. (a) Offset Kirchhoff gather using the Beam Tomography velocity model (left) and the (b) archived Kirchhoff conventional velocity build model.

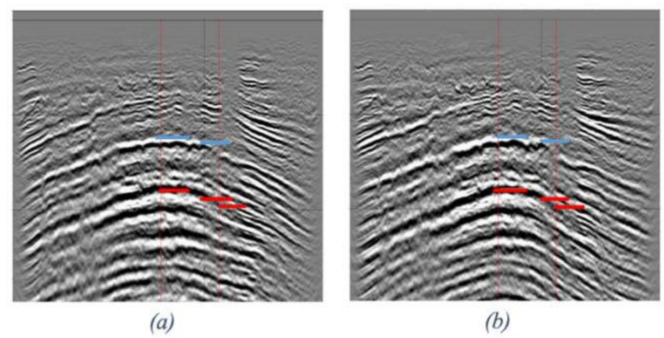

Figure 4. (a) Beam Tomography migrated stack. (b) Archived Isotropic model stack. Blue and red are formation top picked on both stacks.

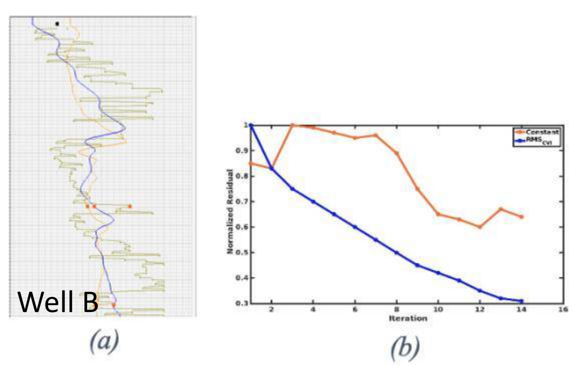

Figure 5. (a) Check-shot (gold). Constant velocity Beam Tomography solution (orange). CVI velocity Beam Tomography solution (blue). (b) L2 norm of the residual update across a single inline per iteration on the constant starting velocity model (orange) and the CVI model (blue).

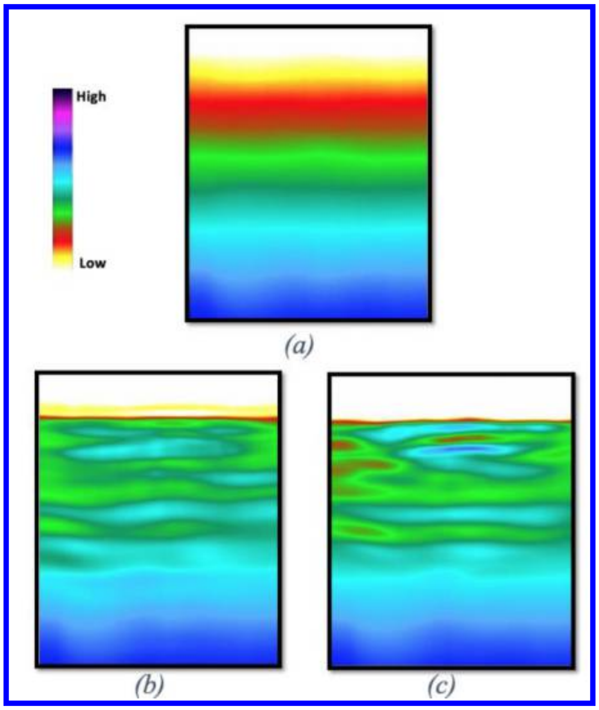

Figure 6. (a) Initial interval velocity model. (b) 9th iteration using the deblended processed data. (c) 10th iteration using the blended data.

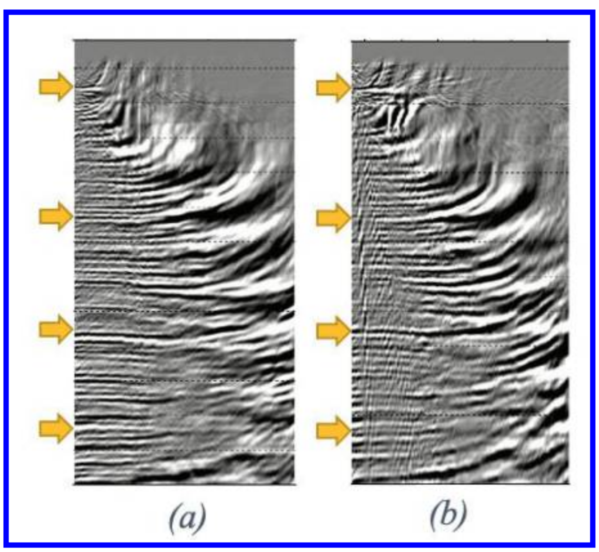

Figure 7. Offset Kirchhoff migration using the velocity model from (a) 9th iteration blended and (b) 10th deblended data.

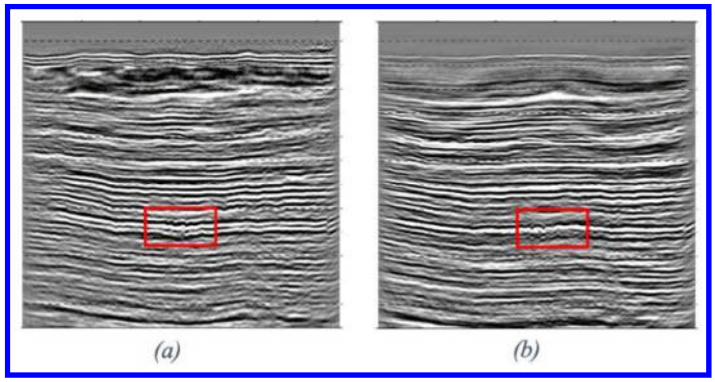

Figure 8. Prestack depth migration stack using (a) Processed deblended data and velocity (Figure 6.b). (b) Raw blended data and velocity (Figure 6.c)

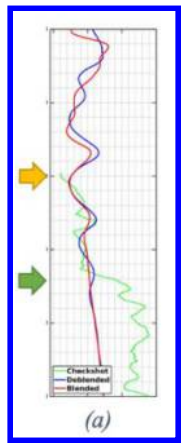

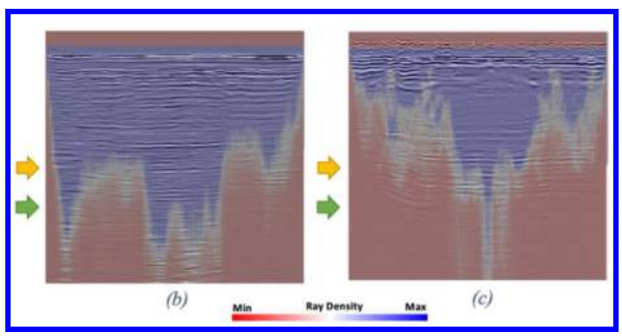

Figure 9. (a) An offset check-shot vs velocity model from deblended and raw blended data. (b) Deblended Beam Tomography stack co-rendered by Beam density. (c) Raw blended Beam Tomography stack co-rendered by Beam density. Arrows indicate point of the same depth on the check-shot and stack.

REFERENCES

Albertin, U., O. Sava, J. Etgen, and M. Mahamrramov, 2006, Adjoint wave-equation velocity analysis: 76th Annual International Meeting, SEG, Expanded abstracts, 3345–3349, doi: https://doi.org/10.1190/1.2370226.

Al-Yahya, K. M., 1989, Velocity analysis by iterative profile migration: Geophysics, **54**, 718–729, doi: https://doi.org/10.1190/1.1442699.

Biondi, B., and P. Sava, 1999, Wave-equation migration velocity analysis: 69th Annual International Meeting, SEG, Expanded Abstracts, 1723–1726, doi: https://doi.org/10.1190/1.1820867.

Červený, V., M. M. Popov, and I. Psencik, 1982, Computation of wave fields in inhomogeneous media Gaussian beam approach: Geophysics Journal International, **70**, 109–128, doi: https://doi.org/10.1111/j.1365-246X.1982.tb06394.x.

Fomel, S., and N. Tanushev, 2009, Time-domain seismic imaging using beams: 79th Annual International Meeting, SEG, Expanded Abstracts, 2747–2752, doi: https://doi.org/10.1190/1.3255419.

Hill, N. R., 2001, Prestack Gaussian-beam depth migration: Geophysics, **66**, 1240–1250, doi: https://doi.org/10.1190/1.1487071.

Richardson, A., and C. Feller, 2019, Seismic data denoising and deblending using deep learning: arXiv:1907.014971v1.

Sava, P., B. Biondi, and J. Etgan, 2005, Wave-equation migration velocity analysis by focusing diffraction and reflection: Geophysics, **70**, no. 3, U19–U27, doi: https://doi.org/10.1190/1.1925749.

Sherwood, J. W. C., K. Sherwood, H. Tieman, R. Mager, and C. Zhou, 2014, Efficient beam velocity model building with tomography designed to accept 3D residuals aligning depth offset gathers: 76th Annual International Conference and Exhibition, EAGE, Extended Abstracts, doi: https://doi.org/10.3997/2214-4609.20141153.

Tanushev, N., A. M. Popovici, and S. Hardesty, 2017, Fast, high-resolution beam tomography and velocity-model building: The Leading Edge, **36**, 140–145, doi: https://doi.org/10.1190/tle36020140.1.

Tarantola, A., 1984, Inversion of seismic reflection data in the acoustic approximation: Geophysics, **49**, 1259–1266, doi: https://doi.org/10.1190/1.1441754.

Tsingas, C., M. Almubarak, W. Jeong, A. Al Shuhai, and Z. Trzesniowski, 3D distributed and dispersed source array acquisition and data processing: The Leading Edge, **39**, 392–400, doi: https://doi.org/10.1190/tle39060392.1.

Virieux, J., and S. Operto, 2009, An overview of full-waveform inversion in exploration geophysics: Geophysics, **74**, no. 6, WCC1–WCC26, doi: https://doi.org/10.1190/1.3238367.

Weber, M., 1988, Computation of body-wave seismograms in absorbing 2-D media using the Gaussian beam method: comparison with extract method: Geophysical Journal International, **92**, 9–24, doi: https://doi.org/10.1111/j.1365-246X.1988.tb01116.x.

10.1190/segam2021-3583236.1